Translational Oncology
www.transonc.com

Volume 10 Number 5 October 2017 pp. 839–845 839

# Spatiotemporal Optoacoustic Mapping of Tumor Hemodynamics in a Clinically Relevant Orthotopic Rabbit Model of Head and Neck Cancer[1]

**Laurie J. Rich*, Sandra Sexton†, Leslie Curtin† and Mukund Seshadri*,‡**

*Laboratory for Translational Imaging, Department of Pharmacology and Therapeutics, Roswell Park Cancer Institute, Buffalo, NY 14263; †Laboratory Animal Shared Resource, Roswell Park Cancer Institute, Buffalo, NY 14263; ‡Department of Oral Medicine/Head and Neck Surgery, Roswell Park Cancer Institute, Buffalo, NY 14263

## Abstract

The purpose of this study was to investigate the usefulness of photoacoustic imaging (PAI) for spatiotemporal mapping of tumor hemodynamics in a rabbit model of head and neck carcinoma. Shope cottontail rabbit papilloma virus associated VX2 carcinomas were established in adult male New Zealand White rabbits ($n = 9$) by surgical transplantation of tumor tissue in the neck. Noninvasive PAI with co-registered ultrasound (US) was performed to longitudinally monitor tumor growth, oxygen saturation (%$sO_2$), and hemoglobin concentration (HbT). PAI findings were validated with Doppler sonography measures of percent vascularity (PV). Differences in tumor volumes, %$sO_2$, HbT, and PV values over time were analyzed using repeated-measures analysis of variance with multiple comparisons. Two-tailed Spearman correlation analysis was performed to determine the correlation coefficient ($r$) for comparisons between %$sO_2$, HbT, and tumor volume. US revealed a significant ($P < .0001$) increase in tumor volume over the 3-week period from 549 ± 260 $mm^3$ on day 7 to 5055 ± 438 $mm^3$ at 21 days postimplantation. Consistent with this aggressive tumor growth, PAI revealed a significant ($P < .05$) and progressive reduction in %$sO_2$ from day 7 (37.6 ± 7.4%) to day 21 (9.5 ± 2.1%). Corresponding Doppler images also showed a decrease in PV over time. PAI revealed considerable intratumoral spatial heterogeneity with the tumor rim showing two- to three-fold higher %$sO_2$ values compared to the core. Noninvasive PAI based on endogenous contrast provides a label-free method for longitudinal monitoring of temporal changes and spatial heterogeneity in thick head and neck tumors.

*Translational Oncology (2017) 10, 839–845*

## Introduction

Photoacoustic imaging (PAI) is an emerging hybrid imaging modality that can provide quantitative readouts of tumor hemodynamics without the need for externally administered contrast agents [1,2]. Unlike traditional radiologic techniques such as computed tomography or positron emission tomography, PAI does not utilize ionizing radiation or radioactive tracers. PAI exploits differences in the optical absorption characteristics of hemoglobin (Hb) depending on its oxygenation state (free versus oxygen bound) to provide quantitative estimates of total Hb concentration and oxygen saturation (%$sO_2$), the amount of oxygen being carried by Hb [3,4]. The reliance of PAI on endogenous contrast along with its short acquisition times makes it particularly attractive for clinical applications in oncology. As such, PAI is being investigated for its diagnostic potential in skin, breast, ovarian, and prostate cancers [5–8]. However, only a few studies have evaluated the utility of PAI based on endogenous contrast for imaging head and neck cancer [9–11]. These published studies of PAI have also been conducted using mouse models of cancer. Murine models are extremely useful for conducting preclinical studies in a time-efficient and cost-effective manner. However, given the ethical considerations and size differences between mice and humans,

Address all correspondence to: Dr. Mukund Seshadri, Roswell Park Cancer Institute, Medical Research Complex, Rm. 232, Elm and Carlton Streets, Buffalo, NY 14263.
E-mail: Mukund.Seshadri@roswellpark.org

[1] Conflicts of interest: The authors do not have any conflicts of interest to disclose. The funding sponsors had no role in the design of the study; collection, analyses, or interpretation of data; writing of the manuscript; and the decision to publish the results.

Received 16 June 2017; Revised 10 August 2017; Accepted 10 August 2017



1936-5233/17
http://dx.doi.org/10.1016/j.tranon.2017.08.004

murine tumor models are limited in their ability to recapitulate thick, bulky human head and neck tumors. In addition to the influence of tumor size on vascularity, thickness of tumors is an important clinical consideration that needs to be recognized while evaluating the performance of optical imaging methods including PAI. In PAI, the imaging depth is limited by light attenuation in tissue that plays a critical role in determining the sensitivity of PAI [12]. It would therefore be important to evaluate the performance of PAI in an animal model that better mimics the clinical scenario in head and neck oncology.

To address this gap in knowledge, in the present study, we 1) developed a novel orthotopic model of the Shope cottontail rabbit papilloma virus associated VX2 carcinoma [13] based on surgical implantation of tumors in the neck of rabbits and 2) examined the ability of PAI to assess spatial and temporal changes in hemodynamics of these bulky VX2 tumors. Noninvasive PAI with co-registered ultrasound (US) was performed to longitudinally monitor tumor growth, $\%sO_2$, and hemoglobin concentration (HbT) *in vivo*. Results obtained with PAI were validated with Doppler sonography–based measures of tumor vascularity.

## Materials and Methods

### *Ethics Statement*

All experimental procedures were performed under aseptic conditions and in accordance with protocols approved by the Institutional Animal Care and Use Committee.

### *Rabbits*

Adult male, specific-pathogen free, New Zealand White (NZW) rabbits (body weight range 1.7-2.6 kg) were purchased from Charles River Corporation (Saint Constant, Quebec, Canada). Animals were allowed to acclimate for 1 week prior to experiments. Rabbits were housed in individual stainless steel cages utilizing noncontact bedding (24" w × 24" d × 16" h) under 12-hour light and dark cycles. Animals were fed high-fiber diet (Rabbit diet # 2031; Harlan Teklad) and purified water. Dietary enrichment consisted of Timothy Hay cubes (Bio-Serv, Flemington, NY) and kale. Environmental enrichment in the form of manipulanda (Bio-Serv, Flemington, NY) was provided to all rabbits.

### *Animal Handling, Anesthesia, and Analgesia*

Prior to surgical or imaging procedures, topical lidocaine and prilocaine anesthetic cream (Hi Tech Pharmacal Co. Inc., Amityville, NY) was applied to the ear. Animals were then sedated using acepromazine maleate (Phoenix Pharm Inc., Burlingame, CA) at a dose of 0.3 mg/kg administered by intravenous injection into the marginal auricular vein. Induction and maintenance of anesthesia were performed using inhalational isoflurane (Patterson Logistics Services Inc., Mount Joy, PA). Preoperative analgesia consisting of 0.05 mg/kg buprenorphine hydrochloride (Patterson Logistics Services Inc., Mount Joy, PA) was administered by intramuscular injection to animals undergoing surgery.

### *VX2 Tumor Propagation and Maintenance*

Frozen tumor pieces were obtained from MD Anderson Cancer Center (Houston, TX). Tissue was homogenized and made into a cell suspension and injected into the thigh muscle of a donor rabbit under anesthesia using an 18-gauge needle. Once the tumor reached ~2.5 cm (typically within 3-4 weeks), the tumor was harvested. Multiple tissue pieces were placed in cryoprotectant media and stored in liquid nitrogen for subsequent use.

### *Surgical Implantation of VX2 Tumors in the Neck*

Surgical procedures were performed in an AAALAC-accredited facility. Naive NZW rabbits were surgically implanted with VX2 carcinoma tumor pieces obtained from a donor rabbit. Following surgical implantation, animals were monitored daily for general health, signs of distress, and tumor growth. Humane end points for euthanasia included tumor size greater than 4 cm in diameter and/or any signs of distress.

### *Photoacoustic Imaging with Co-Registered US*

The setup for PAI with co-registered US of rabbits is shown in Figure 1. Experimental PAI with co-registered US was performed using a laser integrated high-frequency US system (Vevo LAZR; FujiFilm VisualSonics Inc., Toronto, Canada). The system consists of a tunable NIR Nd:YAG laser connected to a 256-element fiber-optic linear array hybrid US transducer, synchronized micro-US system, and a workstation to process and reconstruct the images. Animals were positioned on their back for imaging. Three-dimensional B-mode US images were acquired prior to PAI for tumor volume measurements. PAI data sets were acquired for whole tumor $sO_2$ and Hbt measurements using the following parameters: frequency: 15 MHz, depth: 30.00 mm, width: 32.00, wavelength: 750/850 nm, and acquisition mode: $sO_2$/Hbt. Time gain compensation was applied during PAI studies to adjust for signal loss at increased depths. Three-dimensional Doppler data sets were acquired for measurements of tumor PV using the following parameters: 15 MHz, pulse repetition frequency: 2 kHz, Doppler gain: 40, depth: 30.00 mm, width: 32.00 mm, beam angle: 0°, sensitivity: 5, and wall filter: medium. Animal vitals were monitored continuously during the imaging procedure and following completion of imaging to ensure full recovery. (See Fig. 1.)

### *Image Processing and Data Analysis*

Postprocessing of all imaging data (mice and rabbit) was performed using the Visualsonics workstation suite (VevoLab, ver. 1.7.2). Estimates of $\%sO_2$ and HbT were calculated using the two-wavelength approach. For all studies, % $sO_2$ total values (which represent the average $\%sO_2$ of all pixels including those with a zero/void estimate) are reported. Analysis was performed by tracing a region of interest for the entire three-dimensional region for PAI and Doppler data sets. All color maps representing $\%sO_2$ and Doppler signal were displayed using a color lookup table superimposed on corresponding US images. All measured values were reported as the mean ± standard error of the mean.

### *Sample Sizes and Statistics*

All statistical analyses were performed using Graph Pad Prism version 6.00 for Windows (Graph Pad Software, La Jolla, CA; www.graphpad.com). Measurements of US volume over a 3-week period were obtained for nine rabbits. Whole tumor measurement of $\%sO_2$ and HbT was performed for all nine rabbits. Doppler sonographic assessment of PV was performed on eight rabbits (Doppler data were not acquired for one of the rabbits). Differences in US-based tumor volumes, PAI-based $\%sO_2$, HbT levels, and Doppler-based PV values over time were analyzed using repeated-measures analysis of variance with Tukey's multiple comparisons test. Two-tailed Spearman

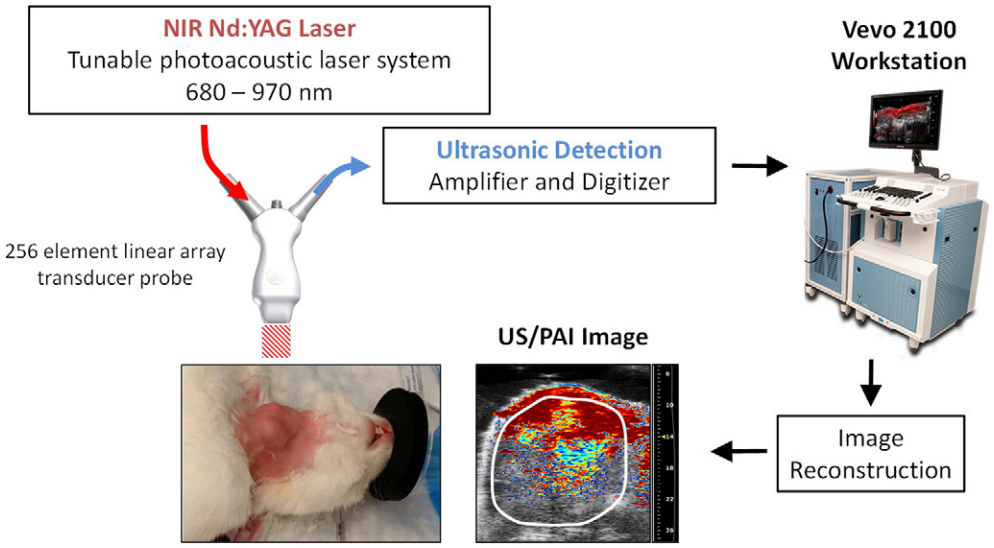


**Figure 1.** Experimental setup for PAI with co-registered US of rabbits bearing orthotopic VX2 tumors. The system consists of a tunable NIR Nd:YAG laser connected to a fiber-optic 256-element linear array hybrid US transducer and processing workstation that creates co-registered PA and US images (Vevo 2100 LAZR; FujiFilm VisualSonics Corporation).

correlation analysis was performed to determine the correlation coefficient ($r$) for comparisons between $\%sO_2$, HbT (PAI), and PV (Doppler) with tumor volume. Subregion analysis of spatial heterogeneity within the tumor was performed in a subset of rabbits ($n$ = 4). Two-tailed paired $t$ test was used to analyze differences in $\%sO_2$, HbT, and PV values between tumor rim and core at different times postimplantation. $P$ values of $< .05$ were considered statistically significant. Values are reported as mean ± standard error of the mean.

## Results

### *Establishing a Clinically Relevant Rabbit Model of Bulky Head and Neck Cancer*

To evaluate the performance of PAI based on endogenous contrast for imaging bulky head and neck tumors, we developed a clinically relevant large animal model of head and neck carcinoma by surgical implantation of Shope cottontail rabbit papilloma virus associated VX2 tumor tissue into the sternohyoid muscle of rabbits as shown in Figure 2. A simplified illustration of the rabbit head and neck anatomy is shown in Figure 2*A*. Using aseptic techniques, the animals were draped, and a 2-cm incision was made on the skin along the length of the neck (Figure 2*B*, *red dotted line*). Delicate blunt dissection of the subcutaneous tissue and fascia was performed. The delicate muscle fibers were separated to create a pocket, and a sterile piece of donor tumor tissue (~2 × 2 mm) was deposited into the pocket created within the lateral aspect of the sternohyoid muscle under anesthesia (Figure 2, *C* and *D*). A 6-0 Vicryl suture was used to close the pocket, and the skin was closed with tissue glue and 5-0 Ethilon suture. The clinical appearance of a rabbit bearing a VX2 tumor in the neck at 3 weeks postimplantation is shown in Figure 2*E*. A total of nine rabbits were surgically implanted with VX2 tumors in the neck as described in "Materials and Methods." All nine animals (100%) survived the surgical procedure without any complications or incidence of postoperative infection. Histologic sections of the tumor exhibited squamous histology along with focal necrotic and hemorrhagic areas (Figure 2*F*).

### *Ultrasonography of VX2 Tumor Growth In Vivo*

All rabbits developed clinically and radiologically detectable tumors within a week postimplantation. Beginning at 7 days postimplantation, US examination was performed at least once a week for 3 weeks. US enabled visualization of the extent of the tumor in all the rabbits ($n$ = 9). Tumors appeared heterogeneous with hypo- and hyperechoic regions visible within the tumor. The panel of images shown in Figure 3*A* represents B-mode US images of a VX2 tumor in the neck of a rabbit at different times (days 7, 14, and 21 postimplantation). Three-dimensional US revealed a significant increase in tumor volume over the 3-week period from 549 ± 260 $mm^3$ on day 7 to 1433 ± 216 $mm^3$ on day 14 ($P < .01$ vs day 7), with tumors reaching a volume of 5055 ± 438 $mm^3$ at 21 days postimplantation (Figure 3*B*, $P < .0001$ vs day 7 and day 14).

### *Temporal Optoacoustic Monitoring of Hemodynamics of VX2 Carcinoma*

We investigated the utility of PAI for evaluation of early- and advanced-stage disease in the orthotopic VX2 rabbit model. To this end, temporal changes in $\%sO_2$ and HbT associated with tumor growth were measured in tumor-bearing rabbits ($n$ = 9). Tumor-bearing animals were imaged once a week for 3 weeks beginning at 1 week postsurgery. At 3 weeks, the depth of the tumors in rabbits was 1.8 ± 0.2 cm. B-mode US images were acquired with co-registered PA maps of $\%sO_2$ and HbT. The panel of images shown in Figure 4A represents PA $\%sO_2$ maps overlaid on the US image (*left*) of a VX2 tumor in the neck. The corresponding Doppler sonographic image of the tumor is shown on the right. The extent of the tumor has been outlined in white on both images. Adequate PA signal was obtained from the tumor in all the animals to obtain measurements of $\%sO_2$ and HbT. PAI revealed a significant ($P < .05$) and progressive reduction in $\%sO_2$ (Figure 4*B*) from day 7 (37.6 ± 7.4%) to day 14 (20.5 ± 5.1%) and day 21 (9.5 ± 2.1%) postimplantation associated with tumor progression over the 3-week period postimplantation. A significant decrease in HbT was also seen during the 3-week period (Figure 4*C*). Corresponding Doppler images showed a decrease in PV over time (Figure 4*D*). A

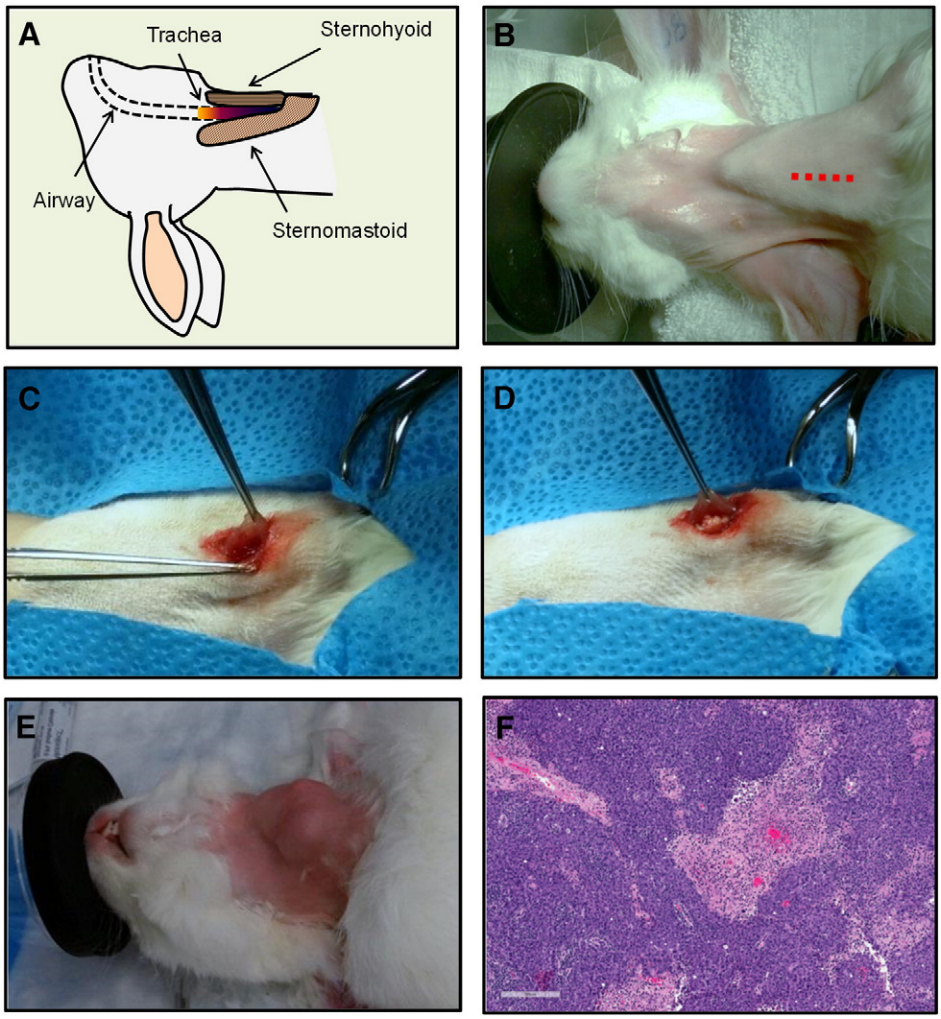


**Figure 2.** Surgical procedure for establishing VX2 carcinomas in the neck of NZW rabbits. (A) Simplified view of rabbit anatomy. (B) Digital photograph of a naive rabbit showing the neck where an incision was made along the length of the dotted red line. (C, D) Subcutaneous tissue dissection and deposition of donor tumor tissue into the sternohyoid muscle. Clinical (E) and histologic (F) appearance of a rabbit bearing orthotopic VX2 carcinoma in the neck.

significant negative correlation ($P < .0001$) was observed between $\%sO_2$ and tumor volume (Figure 4*E*, Spearman $r = -0.80$) and between tumor volume and PV (Figure 4*G*, Spearman $r = -0.72$). A significant relationship ($P = .0004$) was also observed between tumor volume and HbT (Figure 4*F*, Spearman $r = -0.64$).

### *Optoacoustic Mapping of Spatial Heterogeneity in Tumor Oxygenation and Vascularity of VX2 Tumors*

Finally, we examined the spatial differences in $\%sO_2$ and vascularity of VX2 tumors by sampling subregions within the tumor (Figure 5*A*, *left*). Figure 5*A* shows pseudocolorized PA $\%sO_2$

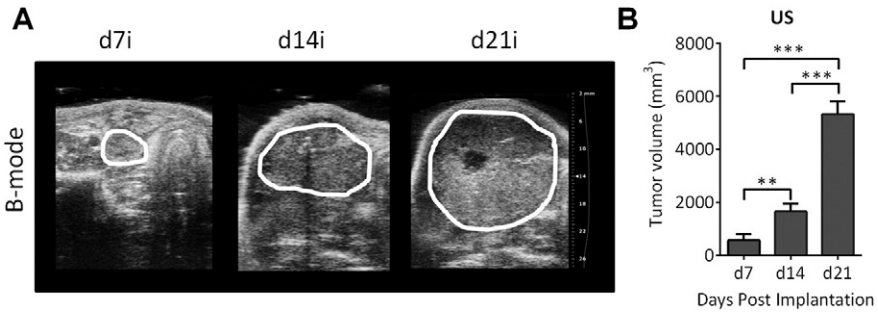


**Figure 3.** Ultrasonography of VX2 tumor growth *in vivo*. (A) B-mode US images of a VX2 tumor in the neck of a rabbit at different times (days 7, 14, and 21 postimplantation). The extent of the tumor is outlined in white. (B) Bar graph shows US-based estimates of tumor volume in rabbits ($n = 9$) over a 3-week period. $^{**}P < .01$; $^{***}P < .001$.

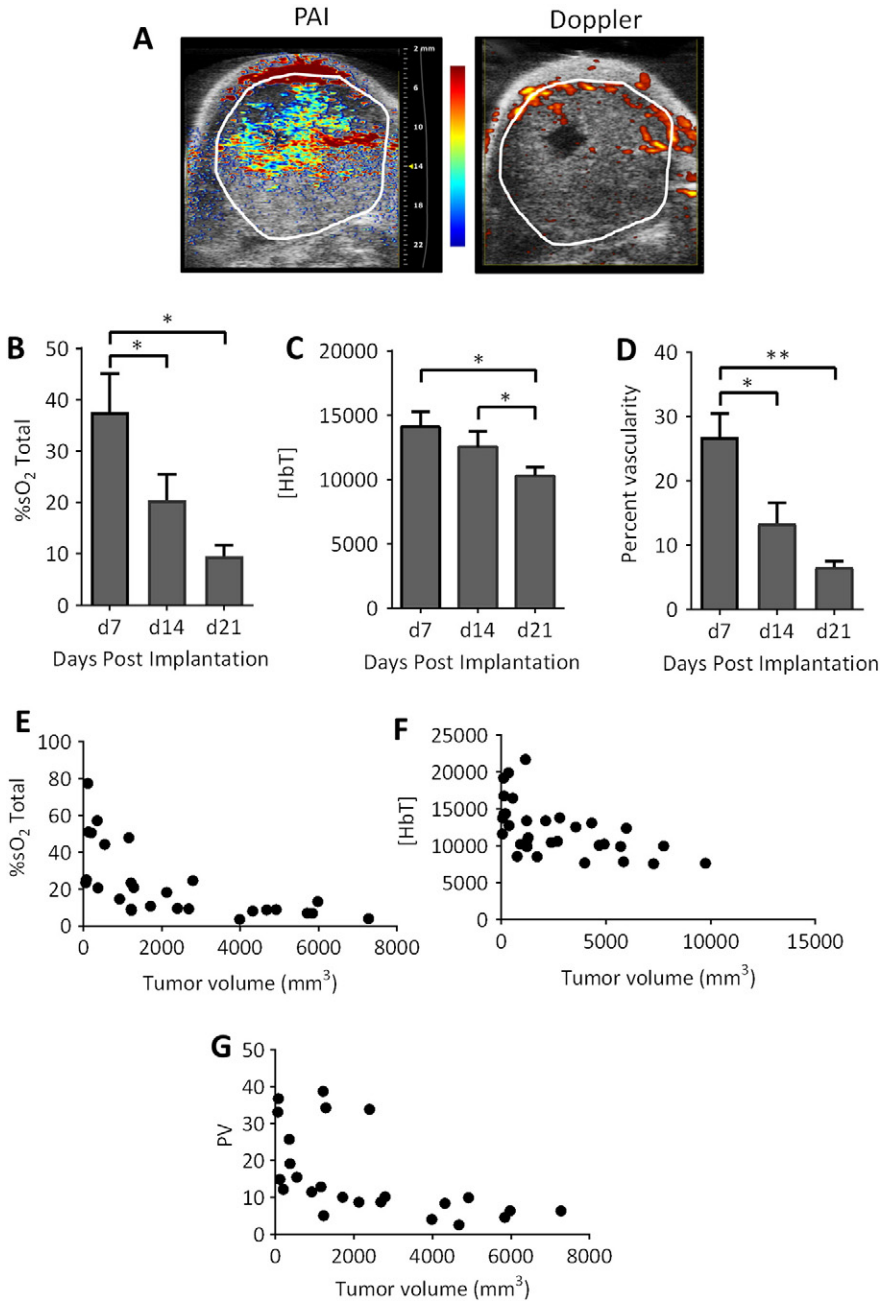


**Figure 4.** Optoacoustic mapping of temporal changes in oxygenation of VX2 rabbit carcinomas. (A) Pseudocolorized PA map of tumor oxygenation saturation overlaid on a B-mode US image of an orthotopic VX2 tumor in a rabbit is shown on the left. Corresponding Doppler image of tumor vascularity is shown on the right. The tumor is outlined in white on both images. Bar graphs show temporal changes in tumor $\%sO_2$ (B) and HbT (C) detected by PAI ($n = 9$). Corresponding values of tumor vascularity (D) on Doppler sonographic examination ($n = 8$) of orthotopic rabbit VX2 carcinomas over a 3-week period. Plots illustrating the correlation between $\%sO_2$ and tumor volume (Spearman $r = -0.80$; $P < .0001$; E), HbT and tumor volume (Spearman $r = -0.64$, $P = .0004$; F), and PV and tumor volume (Spearman $r = -0.72$; $P < .0001$; G). *$P < .05$; **$P < .01$.

map (*middle*) of a VX2 tumor showing considerable heterogeneity in oxygenation within the tumor. Peripheral (rim) regions of the tumor showed consistently higher $\%sO_2$ (Figure 5*B*) and Hbt values (Figure 5*C*) than the tumor center (core). Spatially co-registered Doppler (*right*) images of vascularity validated PA findings. Doppler flow images detected "spots" and strip-like echoes of blood vessels that were restricted primarily to the periphery of the tumor. Consistent with the PAI data, Doppler sonography also showed higher values of vascularity in the tumor rim compared to the core (Figure 5, *A* and *D*). As observed with whole tumor measurements, a progressive reduction in $\%sO_2$ and vascularity was seen with tumor growth over time.

## Discussion

A majority of published preclinical studies have examined the potential of PAI for tumor imaging using superficial tumors in rodent models. Given the depth limitation of PAI, we evaluated the feasibility and performance of PAI for deep tissue imaging of thick tumors in an orthotopic rabbit model of head and neck carcinoma.

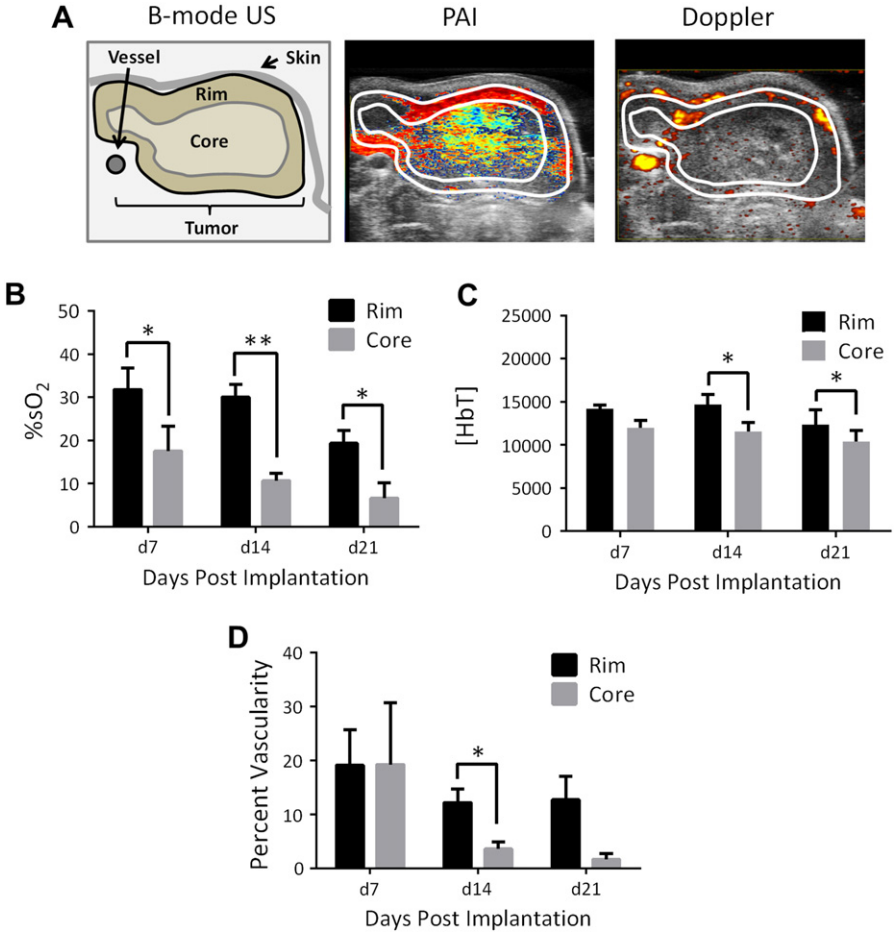


**Figure 5.** PAI and Doppler sonography of spatial heterogeneity in oxygenation and vascularity of VX2 rabbit carcinoma. (A) Pseudocolorized PA $\%sO_2$ and Doppler vascularity maps of a VX2 tumor showing considerable heterogeneity within the tumor. Peripheral (rim) regions of the tumor showed consistently higher values of $\%sO_2$ (B) and HbT (C) than the tumor core. Consistent with the PAI data, Doppler sonography (D) also showed higher values of vascularity in the tumor rim compared to the core. $^*P < .05$; $^{**}P < .01$.

The VX2 Shope papilloma virus associated carcinoma is a widely studied tumor model that has been utilized to evaluate interventional procedures and imaging methods [14–16]. The common sites of tumor implantation in this model include the leg muscle, liver, and auricles [15–17]. Studies have also established VX2 tumors in the buccal mucosa, larynx, and esophagus [18–20]. To mimic thick neck masses seen in humans, we developed an orthotopic neck tumor model by surgically implanting tumor tissue into the sternohyoid muscle of rabbits. The surgical procedure was well tolerated and did not result in any morbidity or mortality. We performed longitudinal US to assess tumor growth in rabbits because high-resolution US is often the imaging method of choice for evaluating neck masses in patients. Tumors were easily detected on US and appeared as well-demarcated masses with heterogeneous echogenicity. US provided evidence of aggressive tumor growth over a 3-week examination period. At late stages of growth, the tumor core appeared anechoic indicative of necrosis.

Whereas the VX2 tumor has been extensively utilized in cancer research, minimal information is available on the temporal and spatial heterogeneity in the oxygenation status of these tumors. Studies have previously examined the potential of PAI for endoscopic imaging of the rabbit esophagus [21] and for ocular imaging in rabbits [22]. Muhanna et al. have previously shown the usefulness of PAI in image-guided therapy of VX2 tumors in the oral cavity using nanoparticle-based contrast agents [23]. In contrast, our study demonstrates the potential of PAI based on endogenous contrast for imaging bulky neck masses in rabbits. We used a commercially available linear array–based PAI system to conduct experimental studies in rabbits. Our studies revealed that PAI can reliably detect hemodynamic parameters up to ~2 cm deep in tissue. With development of next-generation PAI and photoacoustic tomography systems and improvements in light delivery, this could be further improved.

As such, there is widespread interest in the clinical application of PAI. However, only a few studies have performed comparative evaluation of PAI with conventional imaging methods. Recent studies have validated PAI-based hemodynamic assessment of tumors in mice with MRI [11] and contrast-enhanced US [11,24]. In the present study, we compared spatiotemporal changes in hemodynamics assessed by PAI with Doppler sonography, an imaging technique that is clinically utilized for imaging vascularity of neck lesions. In our study, tumor oxygenation assessed using PAI was compared with Doppler measures of vascularity in VX2 neck tumors in rabbits. Good correlation was observed between photoacoustically derived $\%sO_2$ values and PV quantified from Doppler sonography. Sequential PAI

examinations showed a marked decrease in $\%sO_2$ of tumors over time reflective of aggressive tumor growth. The tumor rim consistently exhibited higher oxygenation (PAI) and vascularity (Doppler) compared to the tumor core. The central regions of the tumor appeared hypoxic with minimal PAI signal. Consistent with this finding, tumors exhibited thick rod-like peripheral Doppler signal and decreased signal in the central regions of the tumor. Collectively, our observations demonstrate the ability of PAI to reliably monitor spatiotemporal changes in tumor oxygenation in thick neck tumors. Our results suggest that PAI may serve as a useful imaging tool in conjunction with Doppler sonography for evaluating superficial neck masses.

The limitations of our study need to be recognized. We did not perform histopathologic or immunohistochemical assessment of hypoxia in our rabbit tumor model. This would have provided further validation of our PAI data. Second, given the pilot nature of our studies, we did not examine the changes in tumor oxygenation following therapeutic intervention. Monitoring the spatiotemporal fluctuations in tumor oxygenation before, during, and after therapy would be valuable in determining the prognostic utility of PAI-based oxygenation measurements. In this regard, the clinically relevant, immunocompetent large animal model presented here can serve as a platform for future investigation into the performance of PAI for therapeutic monitoring of chemotherapy, radiation, and immunotherapies. We have begun addressing some of these questions and will report on our findings in the future.

In summary, the work presented demonstrates the ability of PAI to longitudinally monitor tumor oxygenation dynamics and map the spatial heterogeneity of hypoxia in thick head and neck tumors. PAI is a relatively inexpensive, nonradioactive imaging modality that exploits endogenous contrast mechanisms to enable monitoring of spatiotemporal fluctuations in tumor oxygenation *in vivo*. Our work highlights the translational potential of PAI for objective assessment of oxygenation status of bulky head and neck tumors. Our results provide encouraging evidence for additional investigation into the potential of PAI for clinical application in head and neck oncology.

## Acknowledgements

This work was supported by grants from the National Cancer Institute (1R01CA204636), National Center for Research Resources (S10OD010393-01), Roswell Park Alliance Foundation (all to M.S.), and Mark Diamond Research Fund (L.J.R) and utilized shared resources supported by the NCI Cancer Center Support Grant P30CA016156 (Johnson, CS).

## References

[1] Beard P (2011). Biomedical photoacoustic imaging. *Interface Focus* **1**(4), 602–631.
[2] Hu S and Wang LV (2010). Photoacoustic imaging and characterization of the microvasculature. *J Biomed Opt* **15**(1), 011101 [Review].
[3] Oraevsky AA, Jacques SL, and Tittel FK (1997). Measurement of tissue optical properties by time-resolved detection of laser-induced transient stress. *Appl Optics* **36**, 402–415.
[4] Wang LV and Masters BR (2010). Photoacoustic imaging and spectroscopy. *J Biomed Opt* **15**(5), 059901.
[5] Zhou Y, Xing W, Maslov KI, Cornelius LA, and Wang LV (2014). Handheld photoacoustic microscopy to detect melanoma depth in vivo. *Opt Lett* **39**(16), 4731–4734.
[6] Heijblom M, Steenbergen W, and Manohar S (2015). Clinical photoacoustic breast imaging: the Twente experience. *IEEE Pulse* **6**(3), 42–46.
[7] Salehi HS, Wang T, Kumavor PD, Li H, and Zhu Q (2014). Design of miniaturized illumination for transvaginal co-registered photoacoustic and ultrasound imaging. *Biomed Opt Express* **5**(9), 3074–3079.
[8] Dogra VS, Chinni BK, Valluru KS, Joseph JV, Ghazi A, Yao JL, Evans K, Messing EM, and Rao NA (2013). Multispectral photoacoustic imaging of prostate cancer: preliminary ex-vivo results. *J Clin Imaging Sci* **3**, 41. http://dx.doi.org/10.4103/2156-7514.119139.
[9] Luke GP and Emelianov SY (2015). Label-free detection of lymph node metastases with US-guided functional photoacoustic imaging. *Radiology* **277**(2), 435–442.
[10] Levi J, Kothapalli SR, Bohndiek S, Yoon JK, Dragulescu-Andrasi A, Nielsen C, Tisma A, Bodapati S, Gowrishankar G, and Yan X, et al (2013). Molecular photoacoustic imaging of follicular thyroid carcinoma. *Clin Cancer Res* **19**(6), 1494–1502.
[11] Rich LJ and Seshadri M (2015). Photoacoustic imaging of vascular hemodynamics: validation with blood oxygenation level–dependent MR imaging. *Radiology* **275**, 110–118.
[12] Wang LV and Junjie Y (2016). A practical guide to photoacoustic tomography in the life sciences. *Nat Methods* **13**(8), 627–638.
[13] Kidd JG and Rous P (1940). A transplantable rabbit carcinoma originating in a virus-induced papilloma and containing the virus in masked or altered form. *J Exp Med* **71**, 813–838.
[14] Lam MK, Oerlemans C, Froeling M, Deckers R, Barten-Van Rijbroek AD, Viergever MA, Moonen CT, Bos C, and Bartels LW (2016). DCE-MRI and IVIM-MRI of rabbit VX2 tumors treated with MR-HIFU–induced mild hyperthermia. *J Ther Ultrasound* **4**, 9. http://dx.doi.org/10.1186/s40349-016-0052-0 eCollection 2016.
[15] Zhang L, Liu FY, Fu JX, Duan F, Fan QS, and Wang MQ (2014). Hepatic arterial administration of sorafenib and iodized oil effectively attenuates tumor growth and intrahepatic metastasis in rabbit VX2 hepatocellular carcinoma model. *Int J Clin Exp Pathol* **7**(11), 7775–7781.
[16] Lijowski M, Caruthers S, Hu G, Zhang H, Scott MJ, Williams T, Erpelding T, Schmieder AH, Kiefer G, and Gulyas G, et al (2009). High sensitivity: high-resolution SPECT-CT/MR molecular imaging of angiogenesis in the VX2 model. *Invest Radiol* **44**(1), 15–22.
[17] Van ES, Robert RJ, Dullens HF, Van Der Bilt A, Koole R, and Slootweg PJ (2000). Evaluation of the VX2 rabbit auricle carcinoma as a model for head and neck cancer in humans. *J Craniomaxillofac Surg* **28**(5), 300–307.
[18] Lin LM, Chen YK, Chen CH, Chen YW, Huang AH, and Wang WC (2009). VX2-induced rabbit buccal carcinoma: a potential cancer model for human buccal mucosa squamous cell carcinoma. *Oral Oncol* **45**(11), e196–203.
[19] Oak C, Ahn YC, Nam SJ, Jung MH, Hwang SS, Chae YG, Lee HS, Lee KD, Jung MJ, and Chun BK, et al (2015). Multimodal imaging using optical coherence tomography and endolaryngeal ultrasonography in a new rabbit VX2 laryngeal cancer model. *Lasers Surg Med* **47**(9), 704–710.
[20] Huang J, Zhang Y, Zhong H, Fan Z, Jiang G, Shen Y, Song H, Tao Z, and Wang K (2014). Comparison of endoscopic submucosal implantation vs. surgical intramuscular implantation of VX2 fragments for establishing a rabbit esophageal tumor model for mimicking human esophageal squamous carcinoma. *PLoS One* **9**(1), e85326.
[21] Yang JM, Favazza C, Yao J, Chen R, Zhou Q, Shung KK, and Wang LV (2015). Three-dimensional photoacoustic endoscopic imaging of the rabbit esophagus. *PLoS One* **10**(4), e0120269.
[22] Hennen SN, Xing W, Shui YB, Zhou Y, Kalishman J, Andrews-Kaminsky LB, Kass MA, Beebe DC, Maslov KI, and Wang LV (2015). Photoacoustic tomography imaging and estimation of oxygen saturation of hemoglobin in ocular tissue of rabbits. *Exp Eye Res* **138**, 153–158.
[23] Muhanna N, Jin CS, Huynh E, Chan H, Qiu Y, Jiang W, Cui L, Burgess L, Akens MK, and Chen J, et al (2015). Phototheranostic porphyrin nanoparticles enable visualization and targeted treatment of head and neck cancer in clinically relevant models. *Theranostics* **5**(12), 1428–1443.
[24] Bar-Zion A, Yin M, Adam D, and Foster FS (2016). Functional flow patterns and static blood pooling in tumors revealed by combined contrast ultrasound and photoacoustic imaging. *Cancer Res* **76**(15), 4320–4331.